Chapter 1

Hydrogen Storage Materials

1.1 Introduction

Hydrogen has drawn attention as a next-generation energy carrier for mobile and stationary power sources [1]. It has a number of advantages over other chemical energy carriers. First, the energy conversion process is a clean one, with water as the waste product. Second, hydrogen can be produced reversibly by the dissociation of water. Lastly, hydrogen has a large chemical energy density per mass of around $39\,\mathrm{kWhkg^{-1}}$, about three times larger than that of chemical fuels such as liquid carbons [2]. For applications with fuel cell vehicles, hydrogen needs to be stored at high densities . Ideally, it should be contained within a small volume without adding too much additional weight to the vehicle. A driving range of at least 300 miles is considered crucial for the commercial success of a light-duty vehicle. This translates into an on-board storage requirement of 5 kg to 13 kg of hydrogen based on projected future fuel cell efficiencies [3]. Unlike other chemical fuels, however, the intermolecular forces in hydrogen are very weak. At ambient conditions of 20 ℃ and 1 bar, a mass of 1 kg of hydrogen occupies a volume of $11.9\,\mathrm{m^3}$. The goal of hydrogen storage research is to decrease this volume while staying within specific temperature and pressure limits.

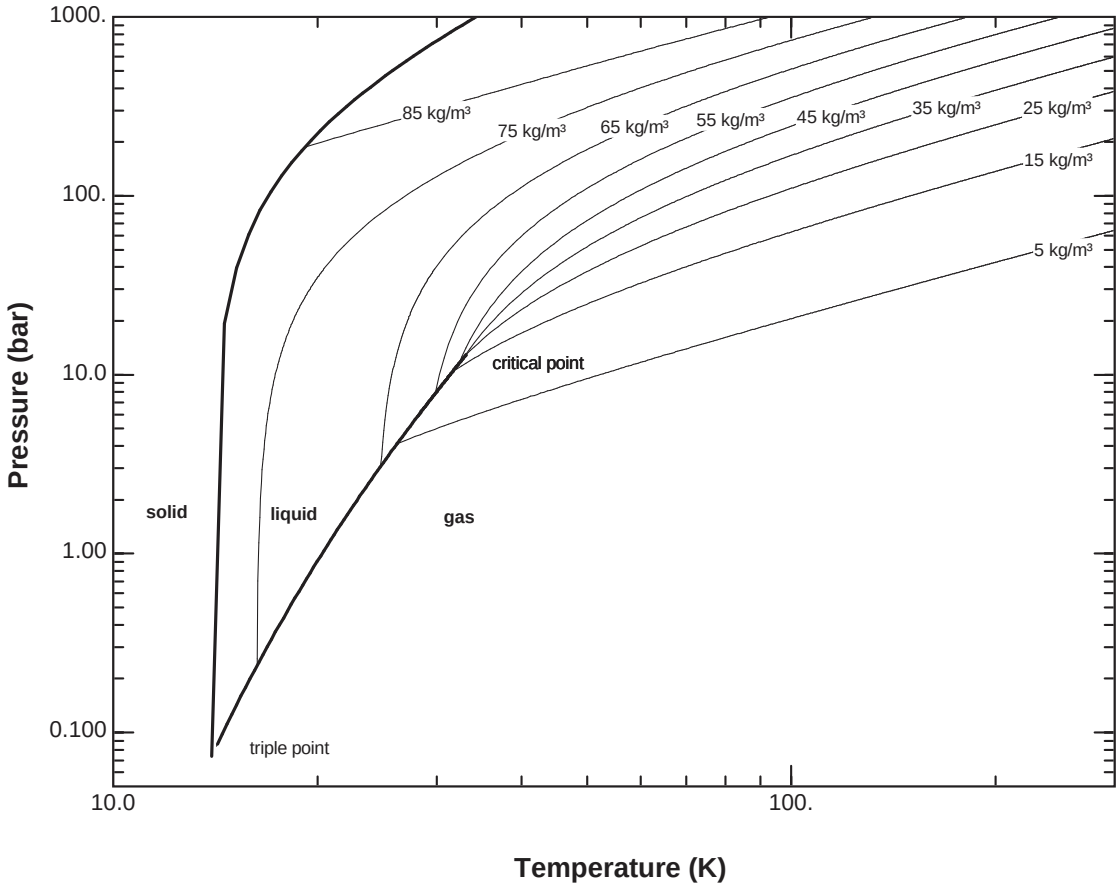

Figure 1.1: Phase diagram for H_2. The melting line and the liquid-vapor line are drawn as bold lines. The triple point and the critical point are both labeled. Constant density contours are drawn as thin lines.

1.2 Physical storage of hydrogen

The fundamental difficulty of storing hydrogen as a liquid or compressed gas is evident in the hydrogen p-T phase diagram shown in Fig. 1.1. At the triple point ($T = 13.803\,\mathrm{K}$, $p = 0.0704\,\mathrm{bar}$) the solid density is $\rho_\mathrm{s} = 86.48\,\mathrm{kg\,m^{-3}}$, the liquid density is $\rho_\mathrm{l} = 77.03\,\mathrm{kg\,m^{-3}}$, and the vapor pressure is a modest 0.07 bar. In the small region between the triple point and the critical point, hydrogen exists as a liquid with a normal boiling point of 20.39 K. If liquid hydrogen is stored in a closed vessel, continuous boil-off can lead to pressures of $10^4\,\mathrm{bar}$. The critical point ($T_\mathrm{c} = 32.98\,\mathrm{K}$, $p_\mathrm{c} = 13.25\,\mathrm{bar}$) of H_2 occurs at a temperature

Table 1.1: Current DOE revised technical targets for on-board hydrogen storage systems for light-duty vehicles

Storage Parameter	Units	2010	2015	Ultimate
System gravimetric capacity[a]	$kg(H_2)/kg(System)$[b]	0.045	0.055	0.075
	kWh/kg	(1.5)	(1.8)	(2.5)
System volumetric capacity	kg/m^3	28	40	70
	kWh/m^3	(900)	(1300)	(2300)
Min/max delivery temperature	K	233/358	233/358	233/358
Cycle life	Cycles	1000	1500	1500
Min delivery pressure	atm	4FC/35ICE[c]	3FC/35ICE	3FC/35ICE
Max delivery pressure	atm	100	100	100
System fill time	kg/min	1.2	1.5	2.0
Fuel purity	Percent H_2		99.99 (dry basis)	

[a] The listed gravimetric and volumetric capacities are *system* targets that include the mass and volume of the system itself, including the tank, material, valves, regulators and other parts. Material capacities may need to be up to twice as large as system capacities. See Ref. [4].
[b] The standard practice here is to define the gravimetric (volumetric) density relative to the maximum final mass (volume) of the combined hydrogen-host system.
[c] FC=fuel cell, ICE=internal combustion engine

which is quite low compared to other gases. Above this temperature hydrogen cannot be liquefied by increasing the pressure. Therefore if the storage system is to operate at higher temperatures, the hydrogen will exist in the gas phase. From the constant density contours in Fig. 1.1, it is clear that at room temperature a pressure of over 1000 bar is required to achieve densities on the order of the liquid or solid phases. This is possible using carbon-fiber-reinforced high-pressure cylinders, but is undesirable for on-board vehicle storage.

1.3 Technical targets for hydrogen storage materials

The U.S. Department of Energy's 2010 and 2015 technical targets for on-board vehicular hydrogen storage are a useful benchmark for comparing different storage methods [4]. Several of the current DOE technical targets are listed in Table 1.1. Operational characteristics such as the temperature, the min/max delivery pressure, the re-filling time, the cycle life, and the fuel purity are also crucial to the performance of the storage system.

Table 1.2: Comparison of hydrogen storage methods

Method	ρ_m (wt%)[a]	ρ_v (kg m^{-3})[b]	T (K)[c]	p (bar)[d]	Description
Compressed gas	13	< 40	273	800	Compressed hydrogen gas; lightweight, high-pressure cylinder
Liquid	Varies	70.8	21.5	1	Liquid hydrogen, continuous loss of a few % per day at RT
Physisorption	≈ 2	20	77	100	Physical adsorption by porous materials, fully reversible
Interstitial metal hydrides	≈ 2	150	273	1	Atomic hydrogen occupies interstitial sites, fully reversible, metals are heavy
Complex hydrides	< 18	150	> 100	1	Complex compounds $[BH_4]^-$ or $[AlH_4]^-$, desorption at elevated temperature, adsorption at high pressure
Chemical hydrides	< 40	> 150	273	1	Thermal decomposition of chemical hydrides, not directly reversible

[a] Gravimetric storage density [b] Volumetry storage density [c] Operational temperatures for storage method
[d] Operational pressures for the storage method [e] Table adapted from Ref. [2]

It is these criteria that make physical adsorption (i.e., physisorption) an attractive storage method. Adsorbed hydrogen does not chemically react during adsorption and, therefore, does not accumulate impurities which can poison the fuel-cell downstream. Because it does not involve bulk solid diffusion or chemical dissociation, the physisorption process is also extremely fast and fully reversible, allowing it to meet both the cycle-life and refilling-time targets. In Table. 1.2, physisorption is compared to the five other basic storage methods. The fundamental problem with physisorption-based storage is that, due to the weak binding interaction between the H_2 and the adsorbent surface, the hydrogen density at ambient conditions is too small.

1.4 Storage based on physisorption

Physical adsorption is a process where gas admolecules bind weakly onto the adsorbent surface by van der Waals (vdW) forces. Chemical bonds are not formed. The equilibrium

adsorption amount $n(T,p)$ is determined by the effective surface area of the adsorbent and the strength of the surface interaction. The adsorbed layer and the bulk gas are in equilibrium so the Gibbs free energies must be equal: $G_{\text{gas}} = G_{\text{ads}}$. Substituting $G = H - TS$ yields

$$H_{\text{ads}} - H_{\text{gas}} = T\left(S_{\text{ads}} - S_{\text{gas}}\right). \tag{1.1}$$

Adsorption involves a reduction in the degrees of freedom of the gas molecules so a tentative assumption $S_{\text{gas}} \gg S_{\text{ads}}$ can be made. For many adsorbents a change in entropy of $-8R$ can be estimated [5]. A simple estimate of the required enthalpy for room temperature storage is

$$\Delta H = H_{\text{ads}} - H_{\text{gas}} \approx -8RT_{\text{room}} = -20\,\text{kJ}\,\text{mol}^{-1}. \tag{1.2}$$

The importance of adsorption thermodynamics can be better illustrated using the Langmuir model.[1] For an equilibrium pressure p, the amount of adsorbed gas is given by

$$n(p) = n_{\max}\left(\frac{Kp}{1+Kp}\right), \tag{1.3}$$

where $n_{\max}$ is the maximum adsorption capacity of the material, and K is the equilibrium constant (which depends on both the temperature and the change in Gibbs free energy). As indicated in Table 1.1, hydrogen should be delivered between a minimum pressure of $p_{\min} = 3\,\text{bar}$ and a maximum pressure of $p_{\max} = 100\,\text{bar}$. The storage system cycles between these operational pressure limits, and the total delivered hydrogen is the difference between $n(p_{\max})$ and $n(p_{\min})$. We want to determine the enthalpy which optimizes the hydrogen delivery between these pressure limits [5]. For an operating temperature of 298 K,

[1] Although the Langmuir model is meant to describe non-interacting adsorbed monolayers on a homogeneous surface, it also works well for describing hydrogen adsorption in microporous materials [6].

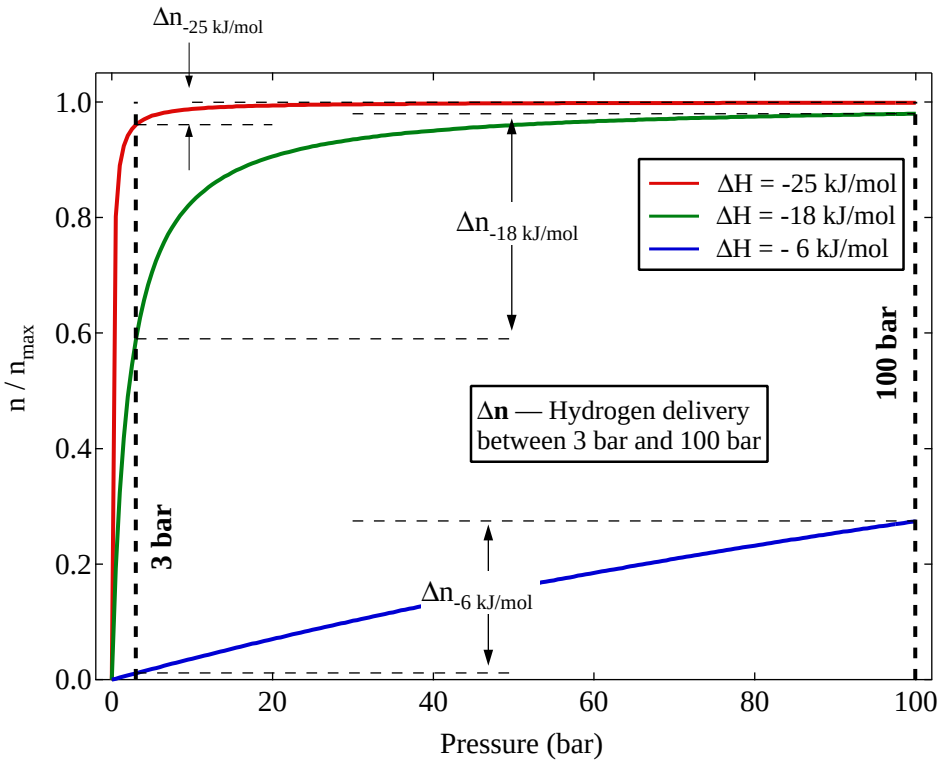

Figure 1.2: Langmuir isotherms for three different adsorption enthalpies (ΔH). Hydrogen delivery (Δn) for each isotherm is indicated by the vertical distance between the adsorption amounts at 3 bar and 100 bar.

realistic estimates of the optimum adsorption enthalpy typically give values around $\Delta H = -18\,\mathrm{kJ\,mol^{-1}}$ [7]. In Fig. 1.2, Langmuir adsorption isotherms are illustrated for various enthalpies of adsorption. It can be seen that the hydrogen delivery depends very strongly on the enthalpy. Because the isotherm for $\Delta H = -25\,\mathrm{kJ\,mol^{-1}}$ is very steep, for example, most hydrogen remains adsorbed when the pressure cycles down to 3 bar. On the other hand, the $-6\,\mathrm{kJ\,mol^{-1}}$ isotherm is very low, containing only a small amount of adsorbed hydrogen at 100 bar. An optimal adsorption enthalpy would occur between these two extremes, providing a larger amount of deliverable hydrogen capacity.

This example demonstrates the importance of *adsorption enthalpy* in determining the properties of a physisorption-based storage system. Because heterogeneous adsorption sites and hydrogen-hydrogen lateral interactions are omitted from the model, the adsorption

enthalpy remains constant as a function of n. But if the constant ΔH is replaced by one that decreases as a function of n, then hydrogen delivery is typically reduced [5]. This makes sense because a single enthalpy can be better optimized than a varying one simply by choosing the optimum enthalpy for every adsorption site. The ideal adsorbent for an isothermal storage system will likely have a constant ΔH of around $-18\,\mathrm{kJ\,mol^{-1}}$, although the specific values will depend on the operational pressure and temperature ranges.

1.5 The mechanism of physisorption

1.5.1 Overview

In Section 1.4 it was illustrated that the enthalpy of adsorption plays a central role in the operational characteristics of a physisorption-based system. To determine the thermodynamic limits of such a storage system a detailed understanding of this interaction energy is critical. Unfortunately, *ab initio* modeling of physisorption is much less developed than it is for chemisorption. The reason is that dispersion forces play a large role in the physisorption mechanism. Although density functional theory works quite well for chemically bound systems, it does not accurately treat long-range interactions of weakly-bound systems [8]. First principles methods capable of treating dispersion forces include the MP2 method (second-order Møller-Plesset perturbation theory) and CCSD(T) method (coupled cluster with single, double, and triple excitations). However these methods are too computationally expensive to apply to realistic adsorbent systems. In fact, empirical potentials are still a starting point for many computational studies of physisorption. In this section, the three main types of hydrogen physisorption interactions will be described.

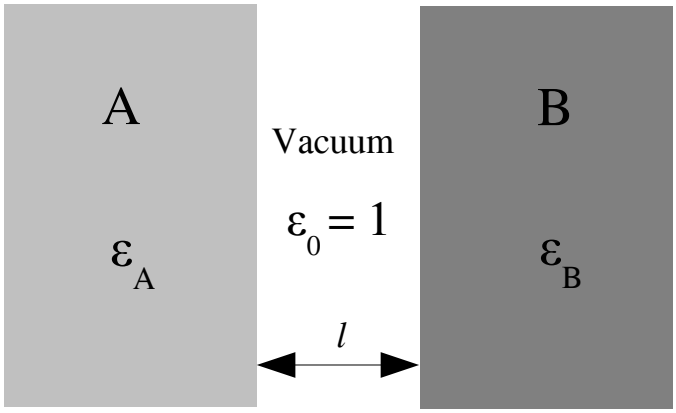

Figure 1.3: Schematic drawing of two semi-infinite slabs of material A and material B with a separation length of l. The region between the two slabs is vacuum. The dielectric constants of the three regions are denoted ϵ_A, ϵ_B and ϵ_0. Adapted from Ref. [9].

1.5.2 Dispersion interactions[2]

A famous example of dispersion forces is provided by the interactions between electrically neutral gas particles which cause deviations from ideal gas behavior at high densities. In brief, dispersion interactions are weak, long-range, nonspecific interactions which are due to charge fluctuations in the two interacting materials. These fluctuations can be due to phenomena such as ionic movements, dipole rotations, and dipole vibrations at the lower frequency end. However, it is the higher frequency electron fluctuations caused by the quantum mechanical uncertainty in position and momentum which contribute most to the interaction. A simple macroscopic system of dispersion interactions between material A and material B across a region of vacuum is illustrated in Fig. 1.3. An electron fluctuating in material A emits an oscillating electric field across the vacuum into material B. This in turn enhances charge fluctuations in material B which lower the overall electromagnetic energy. The mutual fluctuations in material A and material B are not simply random, but have a correlation that affects the total energy and results in a net force. The susceptibility

[2]The analysis presented in this section closely follows Ref. [9].

of each region to the time-varying electric fields, given by the dielectric response ϵ_{A}, ϵ_{B}, itself depends on the frequency of the oscillations. The free energy per unit area required to bring slabs A and B from infinity to a separation l is given by the Hamaker equation,

$$G(l) = \frac{k_{\mathrm{B}}T}{8\pi l^2} \sum_{n=0}^{\infty} d_{\mathrm{A}}(\xi_n)\, d_{\mathrm{B}}(\xi_n)\, R_n(l), \tag{1.4}$$

where the relative difference between the material dielectric responses $\epsilon_{\mathrm{A}}(\xi)$ and $\epsilon_{\mathrm{B}}(\xi)$ and the vacuum dielectric response $\epsilon_0 = 1$ is given by

$$d_{\mathrm{A}}(\xi) = \frac{\epsilon_{\mathrm{A}}(\xi) - 1}{\epsilon_{\mathrm{A}}(\xi) + 1}, \qquad d_{\mathrm{B}}(\xi) = \frac{\epsilon_{\mathrm{B}}(\xi) - 1}{\epsilon_{\mathrm{B}}(\xi) + 1}. \tag{1.5}$$

The relativistic screening term, $R_{\mathrm{n}}(l)$, damps the electron correlations at large distances due to the finite time that the fluctuating electric fields take to reach the other material. Since $R_{\mathrm{n}}(l)$ is only important at large separation distances, it can be ignored for physisorption. The sum in Eq. 1.4 is taken over a discrete sampling of the frequency (ξ_n).[3] The lowest frequencies are on the order of the thermal energy and may originate from vibrations or rotations of polar molecules. However, the sum is dominated by the larger UV and X-ray frequency range.

This macroscopic analysis can be reduced to the familiar point-particle interaction formulas if we assume material A and material B are regions of a dilute gas. In this case $\epsilon = 1 + N\alpha$, where N gives the number density of the dilute gas. The total polarizability

[3]The variable ξ is the imaginary component of the complex frequency, $\omega = \omega_{\mathrm{R}} + i\xi$. Another way to write this is $\exp(i\omega t) = \exp(-\xi t)\exp(i\omega_{\mathrm{R}} t)$. The real frequency, ω_{R}, corresponds to sinusoidal behavior, while the imaginary frequency represents a decaying exponential. The dielectric responses are expressed in terms of a characteristic relaxation time (τ) over which a spontaneous charge fluctuation dies out. For example, the UV and X-ray regions have relaxation times on the order of $\tau \leq 10^{-17}$ sec while molecular vibrations have $\tau \leq 10^{-16}$ sec. When written in terms of the relaxation time, the dielectric response is a smoothly varying curve. This is preferable to the large spikes near resonance that occur when the dielectric response is expressed in terms of ω_{R}.

α of each gas molecule consists of the permanent dipole moment (μ_{dip}) and the inducible polarizability (α_{ind}). If the molecules have a permanent dipole moment, then dipole-dipole (Keesom) and dipole-induced-dipole (Debye) interactions are present. These are the "zero-frequency" electrostatic interactions, given by

$$\text{(Keesom)} \qquad g(r) = -\frac{\mu_{\text{dipole}}^4}{3k_{\text{B}}Tr^6}, \tag{1.6a}$$

$$\text{(Debye)} \qquad g(r) = -\frac{2\mu_{\text{dipole}}^2}{r^6}\alpha_{\text{ind}}(0). \tag{1.6b}$$

The London force is caused by electron correlations at all frequencies. When the retardation screening factor is omitted, this interaction reads as

$$\text{(London)} \qquad g(r) = -\frac{6k_{\text{B}}T}{r^6}\sum_{n=0}^{\infty}\alpha_{\text{ind}}^2(i\xi_n). \tag{1.7}$$

London originally derived the r^{-6} expression in 1930 for two hydrogen atoms at large separation. From accurate first-principles calculations it is known that when hydrogen interacts with large molecules, the energy minimum for the London force occurs at about one molecular radius and has a binding energy on the order of several $\text{kJ}\,\text{mol}^{-1}$ [10]. When the charge distributions overlap at small separations, Pauli repulsion becomes the dominant force; it is typically modeled with a repulsive r^{-12} component in a Lennard-Jones potential.

1.5.3 Electrostatic interactions

The hydrogen molecule does not have a permanent dipole moment. Due to the prolate, non-spherical shape of the H_2 molecule, the first non-zero multipole moment is the quadrupole moment. The ion-quadrupole interaction goes as r^{-3} as a function of distance. Further, the hydrogen molecule is polarizable in the presence of external fields, and the ion-induced-

dipole interaction goes as r^{-4} as a function of distance. For a hydrogen molecule interacting with a unit charge at a distance of 3 Å, the ion-quadrupole interaction energy is about $3.5\,\mathrm{kJ\,mol^{-1}}$ [10]. The associated ion-induced-dipole interaction energy is about $6.8\,\mathrm{kJ\,mol^{-1}}$ [10]. In the presence of a strong external field, it would appear that electrostatic interactions are considerably larger than dispersion interactions. In reality, though, few adsorbent systems actually contain unscreened ionic charges. Even in a first approximation, dispersion forces cannot be ignored for physisorption systems.

1.5.4 Orbital interactions

Molecular hydrogen contains a ground state bonding orbital σ_g with an energy level of about $-11.7\,\mathrm{eV}$. There is a relatively large energy gap between the bonding orbital σ_g and the unoccupied anti-bonding orbital σ_u^* with a magnitude of about 2 eV [10]. Interactions between filled molecular orbitals are primarily repulsive. However interactions between filled and unfilled orbitals can result in charge transfer, donor-acceptor bonding, and overall stabilization. Orbital interactions have shorter bond lengths and larger binding energies than dispersion interactions. Charge transfer causes an elongation of the H_2 bond length, which is directly measurable by a softening of the intramolecular vibrational modes. Transition metals (TM) are known to form H_2 coordination complexes (i.e., "Kubas" complexes) in which H_2-σ to TM-d electron-transfer is coupled with TM-d to H_2-σ^* electron back-donation [11]. In reality, though, hydrogen does not easily donate or accept charge due to the large separation between its σ_g and σ_u^* orbitals. In fact, the adsorption mechanism in many metal-organic frameworks with exposed transition metal sites can actually be explained in terms of electrostatic interactions, without the need for orbital interactions [12].

1.6 Carbon adsorbents

1.6.1 Overview

Carbon adsorbents are attractive for physisorption storage systems due to their simplicity, light weight, and low manufacturing cost. Considerable work has been performed in this field, and at least two review articles are available which describe the status of hydrogen storage in carbon materials [13, 14]. Non-carbon adsorbents which are of particular importance to the hydrogen storage field are described briefly in Sec. 1.6.5.

Nonporous amorphous carbons can be thought of as agglomerates of spheroidal particles. In this case the specific surface area (SSA) consists of the external particle areas, typically in the range of $2\,\mathrm{m^2\,g^{-1}}$ to $200\,\mathrm{m^2\,g^{-1}}$, depending on the particle size. A porous material contains narrow internal cavities or channels which connect to the particle surface. Pore sizes are classified by IUPAC as micropores (pore width $< 2\,\mathrm{nm}$), mesopores (pore width 2–50 nm) and macropores (pore width $> 50\,\mathrm{nm}$) [6]. Microporous carbons are of particular importance for hydrogen storage since they contain large surface areas and provide strong binding sites.

1.6.2 Graphite

Graphite is an ordered carbon allotrope consisting of alternating layers of sp^2 bonded trigonal planer sheets. Neighboring planes interact by overlapping π-bonds between the unhybridized carbon 2p orbitals. The stacking sequence of the basal planes along the c-axis follows a staggered -ABAB- pattern, so that half of the carbon atoms in a given plane sit between the hexagon centers of the layers above and below it.[4] The carbon-carbon bond

[4] Rhombohedral graphite follows an -ABCABC- stacking sequence.

length in the basal planes is $a = 1.421\,\text{Å}$, and the interlayer spacing is $3.354\,\text{Å}$.[5]

Graphitic carbons are nonporous, with surface areas typically under $20\,\text{m}^2\,\text{g}^{-1}$, and negligibly small hydrogen uptake at low temperature [6]. The measured adsorption enthalpy of hydrogen on Graphon[6] is $3.8\,\text{kJ}\,\text{mol}^{-1}$ [15], well below the targeted value. One strategy for increasing the binding energy for carbon adsorbents is to open up space between the layer planes in order to accommodate guest molecules. In fact, this hypothetical graphene slit-pore structure has been the subject of numerous computational studies [16–18]. Due to the overlapping potential fields from opposing slit-pore walls, the heat of adsorption is enhanced. The optimal interlayer spacing would be large enough to accommodate two hydrogen monolayers (i.e., one monolayer per slit pore wall). Any additional interlayer expansion would not be useful because hydrogen only adsorbs in monolayers at supercritical temperatures.

Although the graphene slit pore structure is well-suited for optimizing the carbon-hydrogen binding interaction, the general consensus is that the gravimetric density is intrinsically low due to the geometry. This can be illustrated by considering H_2 monolayers on an ideal graphene sheet. An estimate of the graphene specific surface area is obtained from the fact that a single hexagon contains a net total of two carbon atoms with an area of $1.5\sqrt{3}a^2$. This gives an SSA of $2633\,\text{m}^2\,\text{g}^{-1}$ on double-sided graphene. Two possible configurations for a hydrogen monolayer on a graphene surface are illustrated in Figure 1.4. Commensurate structures are energetically favorable since the hydrogens sit in the hexagon centers, but they have a lower density than a close-packed structure. If both sides of the graphene surface are occupied, then the gravimetric density is 5.6 wt% for the commensurate

[5] This structure corresponds to an ideal graphite crystal, whereas natural graphite contains both hexagonal and rhombohedral modifications, as well as large deviations from the ideal stacking sequence. Natural graphite also contains large amounts of chemical impurities.

[6] Graphon is a graphitized carbon black material with a surface area of $90\,\text{m}^2\,\text{g}^{-1}$ which is typically used as a substitute for graphite in adsorption measurements

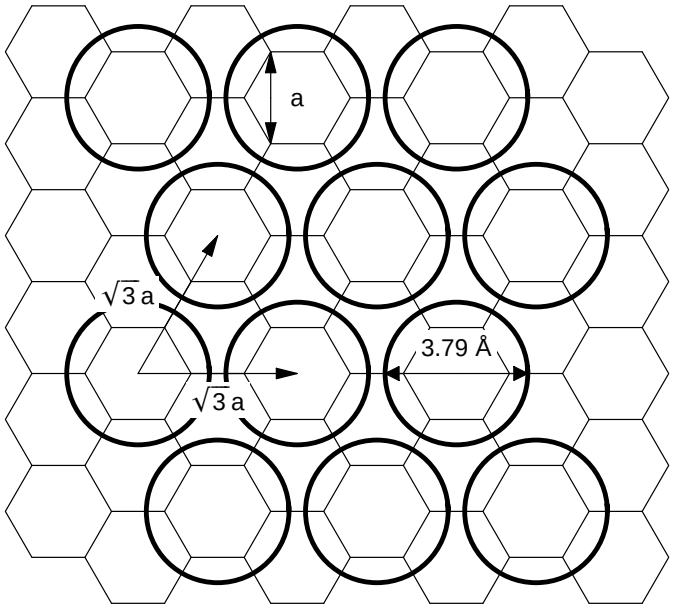

(a) $\left(\sqrt{3} \times \sqrt{3}\right) R30°$

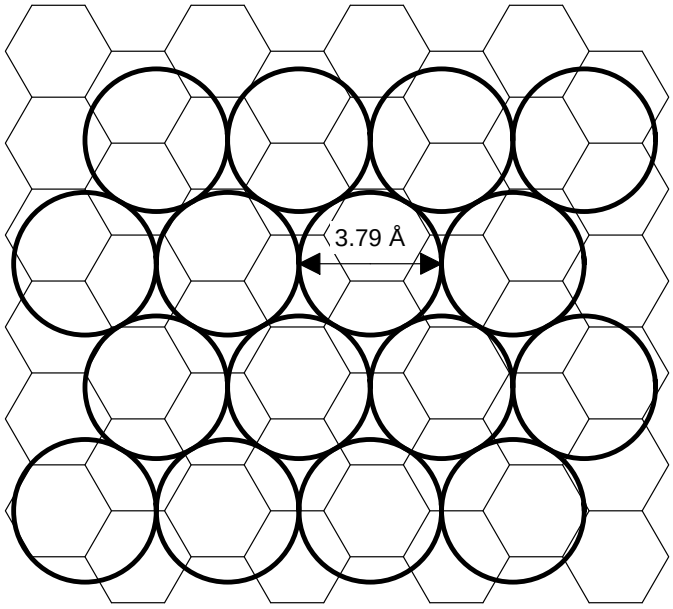

(b) Close-packed

Figure 1.4: Two possible structures for a hydrogen monolayer on a graphene sheet.

$\left(\sqrt{3} \times \sqrt{3}\right) R30°$ structure.[7] The gravimetric density of a close-packed H_2 monolayer can be obtained by using the standard method of estimating the BET cross-sectional area [6]. For a hexagonal close-packed structure, the cross-sectional area of a hydrogen molecule is given by

$$\sigma = f\left(\frac{M}{\rho N_a}\right)^{2/3}, \tag{1.8}$$

where the HCP packing factor f is 1.091, ρ is the density of liquid hydrogen, M is the molar mass, and N_a is Avogadro's number. Taking the solid H_2 density as $\rho = 86.48\,\mathrm{kg\,m^{-3}}$, the cross-sectional area is $\sigma = 0.124\,\mathrm{nm}^2$. If the carbon specific surface area is $a(\mathrm{SSA})$, then the hydrogen monolayer adsorption in wt% is

$$\mathrm{wt\%} = \left(\frac{a(\mathrm{SSA})}{\sigma}\right)\left(\frac{M}{N_a}\right) \times 100. \tag{1.9}$$

This gives $1.34\,\mathrm{wt\%}$ per $500\,\mathrm{m^2\,g^{-1}}$ carbon surface area. Double-sided graphene has a surface area of $a(\mathrm{SSA}) = 2633\,\mathrm{m^2\,g^{-1}}$, which translates to a maximum hydrogen adsorption of $7.04\,\mathrm{wt\%}$. This represents the theoretical limit for H_2 density in a pillared graphene structure.

1.6.3 Fullerenes

Another strategy to enhance hydrogen binding in carbon adsorbents is to use a curved carbon surface. Fullerenes, such as single-walled carbon nanotubes (SWCN) and C_{60} buckeyballs, are well-known examples. They are formed from graphene-like sheets composed of five or six-member rings. The presence of pentagonal rings results in the curvature of the carbon planes, allowing the formation of C_{60} spheres. Similarly, the hollow cylindrical

[7] We can adopt the nearest-neighbor distance of solid hydrogen (3.79 Å) as a conservative estimate of the hard sphere diameter.

structure of single- and multi-wall carbon nanotubes is obtained by rolling up graphene sheets along different directions. Unfortunately, a large amount of variation and irreproducibility has plagued both experimental and theoretical work on hydrogen adsorption in fullerenes. Recent studies have indicated that carbon nanotubes have the same adsorption properties as activated carbons and other amorphous carbons [19, 20]. Nevertheless, as the only ordered allotropes of carbon that adsorb hydrogen, fullerenes provide a unique platform for rigorously studying the hydrogen-carbon interaction from both an experimental and theoretical level. For example, the diameter of the SWCNs is a tunable parameter which can be used to optimize the adsorption behavior.

1.6.4 Activated Carbons

Activated carbons are predominantly amorphous materials with large surface areas and pore volumes, often containing BET areas in excess of $2000\,\mathrm{m^2\,g^{-1}}$. They are best described as "a twisted network of defective carbon layer planes cross-linked by aliphatic bridging groups [21]." The pore structure of an activated carbon is complex and ill-defined, making it challenging to study. An example of this complex, cross-linked structure is illustrated in Fig. 1.5c. Activated carbons are produced in industrial quantities from a carbon-rich precursor by a physical or chemical activation process. Physically activated carbons commonly use bituminous coal or coconut shells as a starting material. The two-stage activation process consists of carbonization, where oxygen and hydrogen are burned off, and gasification where the char is heated in a steam or carbon dioxide atmosphere to create a highly porous structure from carbon burn-off. Carbon aerogels are a separate class of amorphous carbons which can mimic the properties of activated carbons. They are prepared by a sol-gel polymerization process and can be activated using the standard methods.

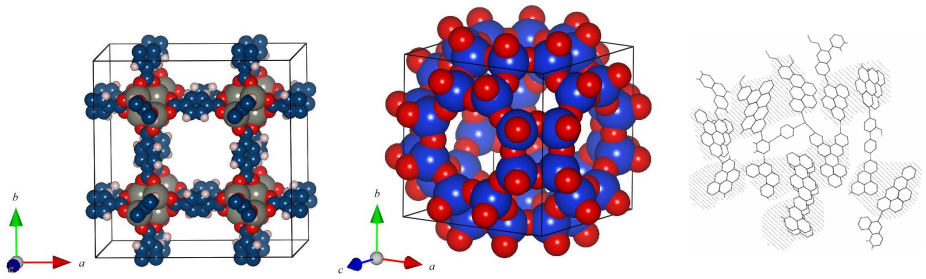

(a) MOF-5 **(b)** Zeolite A **(c)** Activated carbon

Figure 1.5: Structure of (a) MOF-5, (b) zeolite A, and (c) activated carbon.

1.6.5 Zeolites

Zeolites are crystalline materials composed of SiO_4 or AlO_4 building blocks. They contain an intra-crystalline system of channels and cages which can trap guest H_2 molecules. The adsorption capacity of zeolites at 77 K is typically below 2 wt%. A theoretical capacity of 2.86 wt% has been suggested as being an intrinsic geometric constraint of zeolites [22]. Due to this low gravimetric density, zeolites are not typically considered feasible hydrogen storage materials. Isosteric heats on the order of 6–7 $kJ\,mol^{-1}$ are typical for hydrogen-zeolite systems [23]. Zeolite structures such as LTA (see Fig. 1.5b) can have intra-crystalline cavities on the order of the H_2 diameter itself. They function as molecular sieves, blocking adsorption of larger gas molecules by steric barriers. They also exhibit quantum sieving effects on hydrogen isotopes. When confined inside a molecular-sized cavity, the heavier D_2 molecule is adsorbed preferentially over the lighter H_2 molecule due to its smaller zero-point motion [24].

1.6.6 Metal-organic frameworks

Metal-organic frameworks (MOFs) are synthetic crystalline materials which are somewhat analogous to zeolites. Organic linker molecules form the building blocks of MOFs, coordina-

tively binding to inorganic clusters to form a porous framework structure. A good example of a MOF structure is provided by MOF-5, which consists of $Zn_4O(CO_2)_6$ units connected by benzene linkers in a simple cubic fashion (Fig. 1.5a). It was not until fairly recently that MOFs were studied as a potential hydrogen storage material [25]. By modifying the organic linkers, the pore size and effective surface area can be tailored quite effectively. Hydrogen adsorption capacities of up to 7.5 wt% at 77 K have been measured for MOF-177 [26, 27]. A number of MOFs contain coordinatively unsaturated metal centers which are known to enhance hydrogen binding interactions [28]. In most cases this interaction is dominated by electrostatic contributions [12, 29, 30], but the possibility of stronger "Kubas" orbital interactions between the hydrogen and the open metal sites has generated considerable interest.

1.6.7 Hydrogen adsorption by porous carbons

Hydrogen adsorption at supercritical temperatures is characterized by weak interactions between the adsorbed hydrogens. Interactions between the hydrogen and the adsorbent surface are dominant, favoring the formation of adsorbate monolayers. Multilayer formation has a characteristic energy on the order of the hydrogen heat of condensation ($0.9\,\mathrm{kJ\,mol^{-1}}$) and does not occur above the critical temperature. Capillary condensation of H_2 inside large pores or cavities is not possible, resulting in a reduction of the usable pore volume. Therefore, micropores are the most important feature of an adsorbent while mesopores contribute little to the total hydrogen capacity.

Many studies have noted a roughly linear relationship between the BET surface area and the maximum H_2 adsorption capacity at 77 K [20,31]. The simple rule-of-thumb for this behavior is 1 wt% per $500\,\mathrm{m^2\,g^{-1}}$. This can be compared to the 1.34 wt% per $500\,\mathrm{m^2\,g^{-1}}$

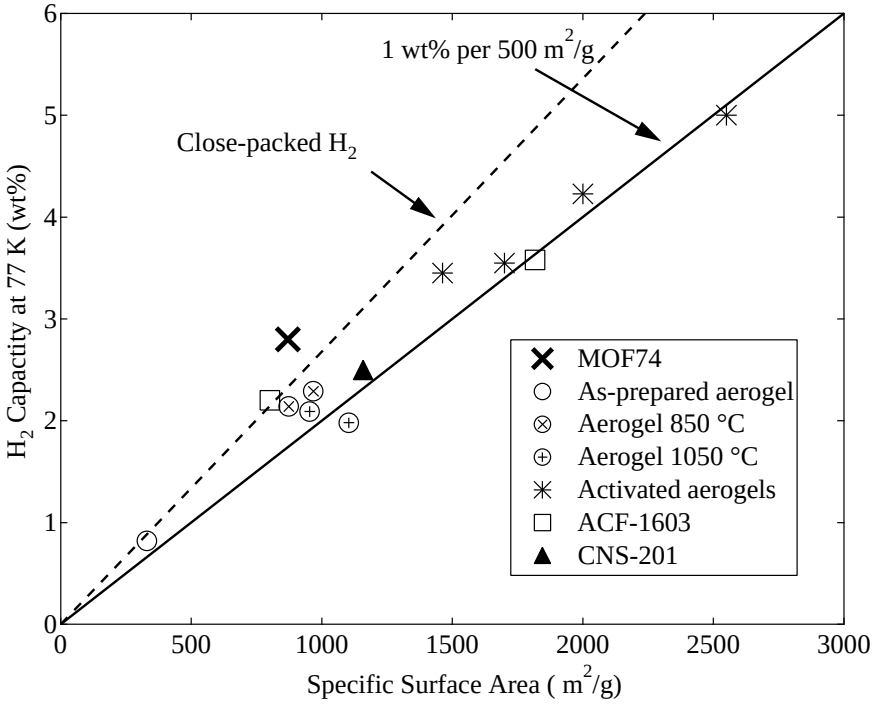

Figure 1.6: Maximum hydrogen adsorption capacities at 77 K of various adsorbents plotted against their BET specific surface areas. Materials include a series of carbon aerogels, two activated carbon fibers (ACF-1603), one activated coconut carbon (CNS-201) and one metal-organic-framework (MOF-74). Straight lines indicate scaling between the specific surface area and storage capacity for close-packed hydrogen and for the rule-of-thumb (1 wt% per 500 $m^2\,g^{-1}$).

obtained for close-packed hydrogen on a double-sided graphene sheet. A sampling of data that was measured in our laboratory is summarized in Fig. 1.6. These samples included carbon aerogels (both activated and as-prepared), activated coconut-shell carbons, activated carbon fibers, and a metal-organic-framework (MOF-74). The scaling between hydrogen capacity and surface area is also plotted for both the empirical rule-of-thumb and the theoretical close-packed limit.

Surface areas do not always have a simple physical meaning for the complex disordered structure of activated carbons. What we should expect, however, is for a correlation to exist between the H_2 uptake and the total *micropore* volume. Studies of both carbon and zeolite adsorbents have found that this type of correlation exists and is actually stronger than the correlation with total BET surface area [19, 32]. In fact, the pore volume obtained from

CO_2 adsorption at 273 K is suggested as better reflecting the total micropore volume due to the faster admolecule diffusion. Hydrogen adsorption is therefore thought to be better correlated to the CO_2 pore volume than to the standard N_2 pore volume [32].

1.6.8 Chemically modified carbon adsorbents

There is a general consensus that carbon adsorbents will not meet density or operational targets for a hydrogen storage system at ambient temperatures [2, 33]. Maximum hydrogen capacity rarely exceeds 1 wt% at room temperature, even at pressures as high as 100 bar [34, 35]. This is an intrinsic property which is due to the low heat of adsorption. It applies equally to carbon nanostructures like SWCNs and to amorphous structures like activated carbons. The most promising strategy for increasing the adsorption enthalpy is through chemical modification of carbon adsorbents.

There are numerous computational studies of hydrogen uptake by hypothetical metal-doped carbon nanostructures. Decoration of C_{60} buckeyballs with scandium [36] or titanium [37] is known to create strong binding sites for multiple H_2 molecules. Metal-decorated SWCNs also exhibit enhanced hydrogen binding energies relative to the pristine material [38]. Computational studies of alkali metal doped graphene and pillared graphite structures have noted the importance of electrostatic effects in enhancing hydrogen binding [39, 40]. Experimental data exists for several metal-doped carbon adsorbents. Potassium-doped activated carbons show enhanced hydrogen adsorption at low pressures relative to the raw material, indicating a larger adsorption enthalpy [41]. Ball-milled mixtures of graphite and potassium adsorb modest amounts of hydrogen between 313 K and 523 K, but the adsorption is not reversible [42].

1.7 Conclusion

The understanding of the effect of chemical modifications on hydrogen adsorption is incomplete. Numerous computational studies exist for hypothetical structures which are not easily synthesized. A large amount of experimental data exists for ill-defined structures such as activated carbons, which are difficult to model theoretically. Research on the fundamental thermodynamics of hydrogen adsorption remains important. In particular, a combination of experimental and computational data on the interaction of hydrogen with a well-defined, chemically-modified carbon adsorbent would provide much needed information. It was for this reason that I chose to study H_2 adsorption in graphite intercalation compounds. This class of materials is introduced in the next chapter.